Polyhedron 29 (2010) 2739–2746

Contents lists available at ScienceDirect

Polyhedron

journal homepage: www.elsevier.com/locate/poly

Self assembly of asymmetric tetranuclear Cu(II) [2 × 2] grid-like complexes and of a dinuclear Ni(II) complex from pyridyl-phenol Schiff base ligands

François Robert [a], Bernard Tinant [a], Rodolphe Clérac [b,c], Pierre-Loïc Jacquemin [a], Yann Garcia [a,*]

[a] Institute of Condensed Matter and Nanosciences, Université Catholique de Louvain, Place Louis Pasteur 1, 1348 Louvain-la-Neuve, Belgium
[b] CNRS, UPR 8641, Centre de Recherche Paul Pascal (CRPP), Equipe "Matériaux Moléculaires Magnétiques", 115 Avenue du Dr. Albert Schweitzer, Pessac, F-33600, France
[c] Université de Bordeaux, UPR 8641, Pessac, F-33600, France

ARTICLE INFO

Article history:
Received 21 April 2010
Accepted 23 June 2010
Available online 30 June 2010

Keywords:
Grid-like complexes
Molecular magnetism
Schiff bases
Self-assembly
Copper(II)

ABSTRACT

Self assembly of *N*-salicylidene 2-aminopyridine (**L1H**) with $Cu(NO_3)_2{\cdot}3H_2O$ affords $[Cu_4(\mathbf{L1})_4(NO_3)_3(CH_3OH)][Cu(\mathbf{L1})(NO_3)_2](2\text{-aminopyridinium})(NO_3){\cdot}5CH_3OH$ (**1**) which is composed of an asymmetric [2 × 2] grid-like cationic complex that co-crystallizes with a Cu(II) mononuclear anion. This remarkable tetranuclear unit presents three penta-coordinated and one hexa-coordinated Cu(II) sites. This quadruple helicate structure reveals strong anti-ferromagnetic coupling ($J = -340(2)\ cm^{-1}$) between Cu(II) ions through a double alkoxo bridge. Reacting **L1H** with $Cu(NO_3)_2{\cdot}3H_2O$ in slightly different conditions affords however a more symmetric tetranuclear grid-like complex: $[Cu_4(\mathbf{L1})_4(NO_3)_2(OH)_2](2\text{-aminopyridinium})(OH){\cdot}CH_3OH$ (**2**). A dinuclear Ni(II) complex, $[Ni_2(\mathbf{L2})_2(\mathbf{L2H})_2(NCS)_2(CH_3OH)_2]{\cdot}2CH_3OH$ (**3**), obtained with another related donor ligand (**L2H** = *N*-salicylidene 3-aminomethylpyridine) was also prepared.

1. Introduction

A major concept in crystal engineering is that covalent blocks can be encoded to interact in a given orientation affording crystal packing control [1]. In such self assemblies, building blocks are directly connected through inter-molecular interactions or by the use of metal ions that can present diverse coordination sphere geometries and natures. Following this synthetic plan, various functional nano-structures (e.g. racks [2], cages [3] and grids [4–7]), which can often reorganize under a given stimulation [8–10], were synthesized. Grid-like metal ion arrays are particularly attractive in this respect for molecular electronic applications because of the well controlled 2D arrangement that can be extended on a given surface [11,12]. In the frame of molecular magnetism, these molecules can behave as single-molecule magnets [13] and be potentially interesting for data storage applications by addressing electronic properties of metal ions (spin state [14], oxidation state [15]). The magnetic properties of [2 × 2] grid-like complexes [16] are relatively rich. In particular, ferromagnetic [17a] and/or anti-ferromagnetic [17] couplings have been observed within and between the supramolecules. High-nuclearity transition metal complexes are also of common interest in bio-inorganic chemistry as they can mimic multimetallic active sites of metalloproteins [18]. A biomimetic application was considered in this context for a Cu(II) [2 × 2] grid-like complex [19]. Thus, the synthesis of asymmetric [2 × 2] nanogrids with different metals [13], spin states [14], coordination spheres [17b] and geometries remains a challenging perspective, particularly in the frame of magnetochirality [20,21]. There exist various ways of generating chiral coordination complexes and assemblies [22,23]. Transfer of chiral information from predesigned optically active ligands or coordination building blocks is generally targeted [24]. This strategy has been successful for developing chiral tetranuclear Cu(II) complexes [25], most examples being found for cubanes [26].

We present herein two new examples of metal directed supramolecular grid self-assemblies using *N*-salicylidene 2-aminopyridine ligand (**L1H**). First, a unique asymmetric [2 × 2] grid-like complex that co-crystallizes with a Cu(II) mononuclear anion: $[Cu_4(\mathbf{L1})_4(NO_3)_3(CH_3OH)][Cu(\mathbf{L1})(NO_3)_2](2\text{-aminopyridinium})(NO_3){\cdot}5CH_3OH$ (**1**). It is a sophisticated architecture comprising not less than three Cu(II) coordination sphere geometries. This asymmetric self-assembly is generated without any ligand conformation asymmetry [27] and affords a strong anti-ferromagnetic (AF) coupling between spin carriers. A more symmetric [2 × 2] grid-like complex was obtained with **L1H** using modified synthetic conditions: $[Cu_4(\mathbf{L1})_4(NO_3)_2(OH)_2](2\text{-aminopyridinium})(OH){\cdot}CH_3OH$ (**2**). A Ni(II) dinuclear complex, $[Ni_2(\mathbf{L2})_2(\mathbf{L2H})_2(NCS)_2(CH_3OH)_2]{\cdot}2CH_3OH$ (**3**), was also prepared with the related Schiff base *N*-salicylidene 3-(aminomethyl)pyridine (**L2H**). It structurally represents half of the [2 × 2] grid-like complex **1** and **2**, and is helpful to understand the complex grid architecture.

* Corresponding author. Fax: +32 1047 2330.
E-mail address: yann.garcia@uclouvain.be (Y. Garcia).

0277-5387/$ - see front matter © 2010 Elsevier Ltd. All rights reserved.
doi:10.1016/j.poly.2010.06.017

2. Experimental

2.1. Starting materials

Solvents (HPLC grade methanol from Prolabo; DMSO-d_6 99.98 atom% D, HPLC grade, *n*-hexane from Aldrich and benzene $\geqslant$99% from Fluka) and reagents (ammonium thiocyanate 99+%, copper(II) nitrate trihydrate 99% and salicylaldehyde 99% from Acros Organics; 3-(aminomethyl)pyridine $\geqslant$99% from Aldrich; 2-aminopyridine 99% from Lancaster; nickel(II) chloride from UCB) were obtained commercially and used as received. *N*-salicylidene 2-aminopyridine (**L1H**) was synthesized following the reported procedure [28].

2.2. Instrumentation

^{1}H and ^{13}C NMR spectra were recorded with a Brüker AC 300 MHz instrument with DMSO as the internal standard. Infrared spectra were recorded with a Shimadzu FTIR-8400S spectrometer with KBr discs. Elementary analyses were performed at University College London. TGA analysis of **1** was made on a Mettler Toledo TGA/SDTA 851e TGA with alumina crucibles filled with approximately 20 mg of sample. Crystalline sample of **1** was taken from the solution and directly sampled under dried air. The temperature program was: (i) isotherm 25 °C, 2 h; (ii) heating to 130 °C, 1 °C/min; (iii) isotherm 130 °C, 1 h; (iv) cooling down to 25 °C, 1 °C/min; (v) stabilization at 25 °C, 5 min; (vi) heating to 450 °C, 10 °C/min. TGA analysis of **3** was made on a TA instrument SDT2960 Simultaneous DSC-TGA with alumina crucibles filled with approximately 10 mg of sample. Approximately 10 mg of dried aluminum oxide were used as reference for DTA measurements. The sample was filtered and stored under dried atmosphere and rapidly measured to avoid moisture absorption. The temperature program was: (i) stabilization at 30 °C; (ii) heating to 150 °C, 1 °C/min; (iii) isotherm 150 °C, 20 min; (iv) cooling down to 25 °C, 1 °C/min; (v) stabilization at 25 °C; (vi) heating to 500 °C, 5 °C/min. Magnetic susceptibility of **1** was measured with a Quantum Design SQUID magnetometer MPMS-XL. *M* vs. *H* measurements were performed at 100 K to check for the presence of ferromagnetic impurities; none were observed. The magnetic data were corrected for the sample holder and diamagnetic contributions. Magnetic susceptibilities of **2** and **3** were not recorded because of the too low available sample quantity of **2** and the likely Curie paramagnetism of **3**.

3. Synthesis

3.1. N-salicylidene 3-(aminomethyl)pyridine (*L2H*)

3-Aminomethylpyridine (2.70 mL) was mixed to benzene (100 mL) in a 250 mL round bottom flask with a Dean–Stark setup that allows trapping water released during condensation reaction. Salicylaldehyde (3.34 mL) was added to give a yellow solution, which was heated at reflux for 24 h. This solution was evaporated and a crude orange oil was isolated. The product was triturated 5× in hexane and a pure solid was filtered and dried under a vacuum line (4.9987 g, 24 mmol, 99%). ^{1}H NMR (300 MHz, [D_6] DMSO, 298 K): 4.85 (s, 2H), 6.92 (m, 2H), 7.35 (m, 2H), 7.49 (dd, J_1 = 1.68 Hz, J_2 = 7.64 Hz, 1H), 7.76 (dt, J_1 = 7.92 Hz, J_2 = 7.89 Hz, 1H), 8.51 (dd, J_1 = 1.56 Hz, J_2 = 4.78 Hz, 1H), 8.60 (d, J_1 = 1.89 Hz, 1H), 8.76 (s, 1H), 13.22 (s, 1H). ^{13}C NMR (300 MHz, [D_6] DMSO, 298 K): 60.67, 117.68, 119.93, 120.01, 124.97, 133.06, 133.79, 135.52, 136.84, 149.76, 150.34, 161.56, 168.36. *Anal.* Calc. (%) for $C_{13}H_{12}N_2O$ (M_t = 212.25 g mol^{-1}): C, 73.57; H, 5.70; N, 13.20. Found: C, 73.12; H, 5.59; N, 12.87%. FTIR (KBr): 1630 (s), 1589 (m), 1491 (m), 1474 (m), 1435 (m), 1389 (w), 1335 (w), 1278 (m), 1259 (m), 1221 (w), 1151 (m), 1117 (w), 1099 (w), 1047 (m), 1007 (w), 893 (w), 839 (w), 802 (m), 754 (s) cm^{-1}.

3.2. [Cu_4(***L1***)$_4$(NO_3)$_3$(CH_3OH)][Cu(***L1***)(NO_3)$_2$](2-aminopyridinium)-(NO_3)·5CH_3OH (***1***)

A solution of Cu(NO_3)$_2$·3H_2O (0.37 g, 1.51 mmol, 4 equiv.) dissolved in methanol (5 mL) was slowly added to a solution of **L1H** (0.3 g, 1.51 mmol, 4 equiv.) dissolved in hot methanol (10 mL). 2-Aminopyridine (0.04 g, 0.4 mmol, 1 equiv.) dissolved in methanol (5 mL) were then added to the mixture to give a dark green solution which was kept in darkness and under a diethyl ether saturated atmosphere over few weeks. A crystalline sample, constituted by a large number of green crystalline blocks, was obtained (0.16 g, 0.08 mmol, 21%). It was essential to control the ether diffusion rate to obtain large single crystals. *Anal.* Calc. (%) for [Cu_4(**L1**)$_4$(NO_3)$_3$(CH_3OH)][Cu(**L1**)(NO_3)$_2$](2-aminopyridinium)-(NO_3)·CH_3OH·6H_2O: $C_{67}H_{77}N_{18}O_{31}Cu_5$ (M_t = 1948.18 g mol^{-1}): C, 41.31; H, 3.98; N, 12.94. Found: C, 40.93; H, 3.05; N, 12.55%. This analysis reveals that four non coordinated methanol molecules have been replaced by six water molecules, provided the samples are stored in air. Indeed, a perfect match is obtained between TGA and X-ray analyses when fresh crystals are quickly transferred from the mother solution to the thermogravimetric analyser. TGA weigh lost at onset temperatures: 25 °C, −1.1%, −1 CH_3OH; 122 °C, −3.8%, −2 CH_3OH; 130 °C, −2.7%, −3 CH_3OH; degradation temperature: 218(1) °C. FTIR (KBr): 3366 (l, s), 1763 (w), 1666 (m), 1601 (s), 1568 (m), 1545 (s), 1481 (m), 1470 (s), 1435 (s), 1385 (s), 1306 (m), 1290 (s), 1267 (m), 1200 (s), 1155 (m), 1128 (w), 1065 (w), 1036 (w), 1022 (w), 989 (w), 933 (w), 864 (m), 825 (w), 806 (m), 783 (w), 762 (m), 741 (w), 675 (w), 646 (w), 627 (w), 598 (w), 555 (m), 538 (w), 521 (w), 465 (w) cm^{-1}.

3.3. [Cu_4(***L1***)$_4$(NO_3)$_2$(OH)$_2$](2-aminopyridinium)(OH)·CH_3OH (***2***)

A solution of Cu(NO_3)$_2$·3H_2O (0.37 g, 1.51 mmol, 5 equiv.) dissolved in methanol (5 mL) was slowly added to a solution of **L1H** (0.3 g, 1.51 mmol, 5 equiv.) dissolved in hot methanol (10 mL). 2-Aminopyridine (0.03 g, 0.3 mmol, 1 equiv.) dissolved in methanol (5 mL) were then added to the mixture to give a dark green solution which was kept in darkness and under a diethyl ether saturated atmosphere over few weeks. A single crystal of **2** was isolated on the glassware and rapidly taken out from the mother solution to be measured by X-ray diffraction. The presence of free hydroxide and 2-aminopyridinium groups in the structure is proposed because such molecules are consistent with the composition of **1** but the possibility to have free water and 2-aminopyridine cannot be excluded.

3.4. [Ni_2(***L2***)$_2$(***L2H***)$_2$(NCS)$_2$(CH_3OH)$_2$]·2CH_3OH (***3***)

$NiCl_2$ (0.056 g, 0.24 mmol, 1 equiv.) was dissolved in methanol (5 mL) and added to a solution of NH_4NCS (0.036 g, 0.47 mmol, 2 equiv.) dissolved in methanol (5 mL). The resulting blue-green solution was then added to **L2H** (0.2 g, 0.94 mmol, 4 equiv.) dissolved in methanol (7 mL). A yellow precipitate (17 mg of crude product) was filtered and the resulting clear green solution was kept over one month in darkness. Complex **3** (0.08 g, 0.07 mmol, 58%) was obtained as green single crystals. *Anal.* Calc. (%) for [Ni_2(**L2**)$_2$(**L2H**)$_2$(NCS)$_2$(CH_3OH)$_2$]·2CH_3OH·H_2O: $C_{56}H_{56}N_{10}O_7S_2Ni_2$ (M_t = 1162.64 g mol^{-1}): C, 57.8; H, 4.85; N, 12.05; S, 5.52. Found: C, 57.50; H, 4.55; N, 12.22; S, 5.61%. TGA weigh lost at onset temperatures: 46 °C, −4.2%, −1.5 CH_3OH; 69 °C, −6.3%, −2.3 CH_3OH; degradation temperature: 169(1) °C. FTIR (KBr): 1624 (s), 1533 (w), 1479 (w), 1468 (m), 1452 (m), 1429 (m), 1400 (w), 1348

(w), 1329 (w), 1279 (w), 1215 (w), 1190 (m), 1126 (w), 1117 (w), 1036 (w), 984 (w), 903 (w), 841 (w), 806 (w), 756 (m), 706 (m) cm^{-1}.

4. Single crystal X-ray diffraction studies

The intensity data were collected at 120 K for **1** and **2**, and at 115 K for **3** with a MAR345 image plate using Mo Kα (λ = 0.71069 Å) radiation. The crystal was mounted in inert oil and transferred quickly to the cold gas stream for flash cooling. Crystal data, data collection parameters, details of the refinement and the final *R* indices are summarized in Table 1. The unit cell parameters were refined using all collected spots after the integration process. The data were not corrected for absorption but the data collection mode partially takes the absorption phenomena into account. The structures **1**–**3** were solved by direct methods with SHELXS97 [29]. All the structures were refined by full-matrix least-squares on F^2 using SHELXL97 [29]. All the non-hydrogen atoms were refined with anisotropic temperature factors and hydrogen atoms were calculated with AFIX. The H atoms were included in the refinement with a common isotropic temperature factor. Some H atoms of solvent molecules could not be localized. Constraints and geometrical parameters of some disordered solvent molecules were applied.

5. Results

5.1. Synthesis

Reacting $Cu(NO_3)_2{\cdot}3H_2O$, **L1H** and 2-aminopyridine in a 4:4:1 ratio in methanol afforded large green blocks of $[Cu_4(\mathbf{L1})_4(NO_3)_3(CH_3OH)][Cu(\mathbf{L1})(NO_3)_2](2\text{-aminopyridinium})(NO_3){\cdot}5CH_3OH$ (**1**). These crystals transform to powder after filtration in air. This behaviour originates from the lost of lattice solvent methanol molecules as concluded from thermogravimetric and elemental analyses. Crystals thus had to be directly taken out from the mother solution and quickly transferred to a diffractometer to enable a crystal structure determination that revealed an interesting [2 × 2] grid-like complex. Surprisingly, reacting $Cu(NO_3)_2{\cdot}3H_2O$, **L1H** and 2-aminopyridine in a different ratio (5:5:1) also in methanol afforded $[Cu_4(\mathbf{L1})_4(NO_3)_2(OH)_2](2\text{-aminopyridinium})(OH){\cdot}{\cdot}CH_3OH$ (**2**) whose crystal structure was determined. Although we assume that its crystal structure is not representative of the major reaction product, it is discussed below because, like **1**, it is a [2 × 2] grid-like complex, and confirms the formation of such self-assembled architecture in the reaction scheme. Note that, in both cases, 2-aminopyridinium acted as a seeding agent. Indeed, all crystallization attempts without this molecule failed whatever the method employed. Single crystals of $[Ni_2(\mathbf{L2})_2(\mathbf{L2H})_2(NCS)_2(CH_3OH)_2]{\cdot}2CH_3OH$ (**3**) were obtained by reacting $NiCl_2$, NH_4NCS and **L2H** in a 1:2:4 ratio in methanol.

Table 1
Crystal data and structure refinement for **1**–**3**.

Compound	**1**	**2**	**3**
Empirical formula	$C_{71}H_{76}Cu_5N_{18}O_{29}$	$C_{60}H_{64}Cu_4N_{14}O_{16}$	$C_{57.5}H_{60}N_{10}O_{7.5}S_2Ni_2$
Formula weight	1963.20	1491.42	1192.70
T (K)	120(2)	120(2)	115(2)
Crystal system	Triclinic	Orthorhombic	Triclinic
Space group	$P\bar{1}$	*Pbcn*	$P\bar{1}$
a (Å)	15.002(2)	14.139(5)	13.639(4)
b (Å)	15.894(5)	24.896(7)	14.517(4)
c (Å)	17.764(3)	16.452(5)	15.404(4)
α (°)	70.20(2)	90	68.32(2)
β (°)	87.83(2)	90	87.47(2)
γ (°)	81.25(2)	90	81.35(2)
V (Å^3)	3938(2)	5791(3)	2802(1)
Z	2	4	2
ρ_{calc} (mg m^{-3})	1.655	1.711	1.413
F(0 0 0)	2010	3064	1246
μ (mm^{-1})	1.425	1.536	0.809
Crystal size (mm)	0.2 × 0.2 × 0.2	0.5 × 0.2 × 0.2	0.4 × 0.1 × 0.1
θ_{max} (°)	24.40	23.55	24.42
Reflections collected/unique	79617/12257	29887/4280	27850/8730
R_{int}	0.046	0.069	0.052
R_1 [$I > 2\sigma(I)$]	0.0424 [10535]	0.0898 [3611]	0.0397 [7501]
wR_2	0.1104	0.2772	0.1060
Largest peak and hole	1.16 and −0.70	1.86 and −1.29	0.42 and −0.41

5.2. Structural aspects

5.2.1. Crystal structure of *1*

The asymmetric part of the unit cell of **1**, which crystallizes in the triclinic space group $P\bar{1}$, is crowded. It contains a non-centrosymmetric cationic Cu(II) [2 × 2] grid-like complex with 4 copper ions labelled as Cu^i (*i* = 1–4), an anionic Cu(II) mononuclear unit, several uncoordinated species (five methanol molecules and one nitrate anion), as well as a disordered 2-aminopyridinium cation, required to ease crystallization (Fig. 1). The coordination sphere of the anionic mononuclear entity around Cu5, $[Cu(\mathbf{L1})(NO_3)_2]$, contains one **L1** and two bidentate nitrato anions. Interestingly, **L1** appears to be twisted (the dihedral angle between salicyl and pyridine rings, Φ = 42(1)°) even though the pyridine moiety is not involved in the coordination sphere. In order to simplify the discussion of the tetranuclear complex, structurally different ligands have been labelled as L*j* (*j* = a–e) (Table 2). Relevant bond length differences and angles are given in Table 3. The coordination sphere of Cu1 is built of five atoms in a square pyramidal geometry which is confirmed by the Addison structural index [30], τ = 0.35. It involves O16 of a monodentate nitrate, N1 from the pyridine of **L1a**, N107 from the imine function of **L1b**, O115 and O215 from alcoholate functions of **L1b** and **L1c**, respectively (Fig. 2). Interestingly, Cu2 adopts a distorted hexa-coordinated coordination sphere with O116 and O119 from a bidentate nitrato anion, N301 from the pyridine of **L1d**, N207 from the imine function of **L1c**, O115 and O215 from alcoholate functions of **L1b** and **L1c**, respectively. The coordination sphere of Cu3, also displayed in Fig. 2, resembles the one of Cu1. It is also penta-coordinated (τ = 0.04) but the nitrato anion has now been replaced by a methanol molecule. Indeed, we find one oxygen atom arising from a methanol molecule (O20), N201 from the pyridine of **L1c**, N307 from the imine function of **L1d**, O15 and O315 from the alkoxo groups of **L1a** and **L1d**. As Cu1, Cu4 also presents a square pyramidal coordination sphere (τ = 0.40) made with O216 from a monodentate nitrato anion, N101 from the pyridine of **L1b**, N7 from the imine function of **L1a**, O15 and O315 from alkoxo groups of **L1a** and **L1d**. However, their connection through μ_2-alkoxo groups to different copper ions (Cu2 and Cu3), makes Cu1 and Cu4 different from a crystallographic point of view (Table 3). The whole [2 × 2] grid forms a slightly distorted square (Fig. 1) with Cu···Cu distances of 3.064(3) Å, 3.067(3) Å, 3.253(3) Å and 3.343(3) Å (Table 2) which are in the same range than the distances observed for $[Cu_4(\mathbf{L1})_4(H_2O)_4](NO_3)_4$ (**4**) [31]. The tetranuclear unit can be viewed as a pair of dinuclear complexes [33], the bridging geometry within each dinuclear unit being made of two μ_2-alkoxo groups with Cu–O–Cu angles around 101.8–102.8° (Table 3) that suggest strong AF interactions between metal ions. Both dimers are linked by two N–C–N bridges including the imine and pyridine moieties of **L1** (Fig. 3). A racemic mixture of two enantiomers, generated by the

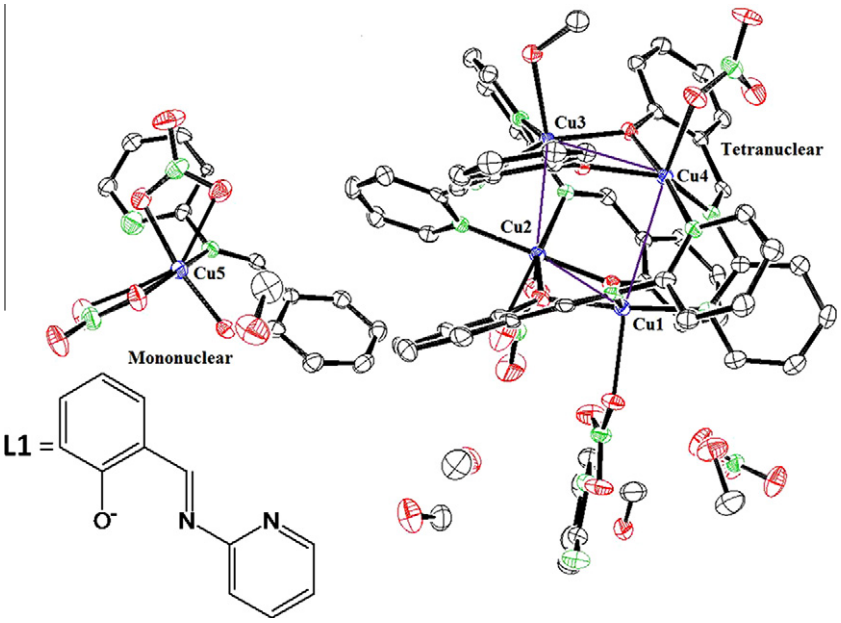

Fig. 1. ORTEP view of the asymmetric part of the unit cell for **1**, showing 50% probability displacement ellipsoids. The Cu^{II} grid-like complex (violet square) is shown on the right side and the mononuclear unit on the left side. H atoms were omitted for clarity. The inset shows a scheme of the **L1** ligand.

Table 2
Selected angles (°) and distances (Å) for **1**–**3**.

Φ[a] (°)	L1a	L1b	L1c	L1d	L1e
1	48(1)	48(1)	42(1)	35(1)	42(1)
2	35(1)	40(1)	–	–	–
3	60(1)	76(1)	90(1)	69(1)	–
C7–N8–C9–C10[b] (°)					
3[c]	125(1)	97(1)	109(1)	126(1)	–
$d_{Himine-H\beta}$ (Å)					
1	2.52(5)	2.48(5)	2.38(5)	2.36(5)	2.33(5)
2	2.34	2.38	–	–	–
3	2.41(2)	2.44(2)	2.43(2)	2.52(2)	–
$d_{M\cdots M}$ (Å)	Cu1–Cu2	Cu2–Cu3	Cu3–Cu4	Cu4–Cu1	Cu2–Cu5
1	3.064(3)	3.253(3)	3.067(3)	3.343(3)	9.082(3)
2	3.067(9)	3.213(9)	–	–	–

[a] Dihedral angle between phenolic and pyridine aromatic rings.
[b] Torsion angle involving the CH_2 spacer group between the imine function and the pyridine ring.
[c] Concerns either **L2Ha**, **L2b**, **L2c** and **L2Hd**.

$P\bar{1}$ symmetry, has been crystallised with a right hand helicate (Δ enantiomer) or a left hand helicate (Λ enantiomer) (Fig. 4) [32]. This situation results from the large twist of **L1** (see torsion angles in Table 1). A dense supramolecular network is also revealed based on 14 inter-molecular H-bonds, one N–H···π and two C–H···π interactions (Table S1).

*5.2.2. Crystal structure of **2***

Complex **2** crystallizes in the orthorhombic space group *Pbcn* and contains a Cu(II) tetranuclear unit, made with **L1**, that forms a [2 × 2] grid-like arrangement with Cu···Cu distances of 3.067(9) Å and 3.213(9) Å (Fig. 5). Two different coordination spheres are identified. Cu1 presents a square pyramidal geometry (τ = 0.40) made of a monodentate nitrato anion (O202) in apical position, two oxygen atoms originating from alkoxo groups of **L1a** (O15) and **L1b** (O115), a nitrogen N1 of the pyridine of **L1a** and a nitrogen N107 of the imine function of **L1b**. Cu2 which is also pentacoordinated presents a similar coordination sphere (τ = 0.01) with a hydroxide (O20) in apical position, two oxygen atoms from alkoxo functions of **L1a** (O15) and **L1b** (O115), a nitrogen N101 of the pyridine of **L1b** and a nitrogen N7 of the imine function of **L1a**. The bridge between Cu ions is ensured, like in **1**, by two alkoxo groups in one direction and by an imine and a pyridine group (N–C–N bridge) in the other direction. Even if only two Cu ions are present in the asymmetric part of the unit cell, the grid-like complex is generated by symmetry. Each ligand **L1** is coordinated to three Cu ions. Interestingly, the coordination involves a large dihedral angle Φ between aromatic rings of **L1** (Φ_a = 35(1)° and Φ_b = 40(1)°) (Table 1). Because of this angle, as in **1**, a quadruple helicate is formed within this chiral tetranuclear unit. The two enantiomers, that crystallize in a racemic mixture, are generated by symmetry in the *Pbcn* group.

The [2 × 2] grid unit also co-crystallizes with a hydroxide ion, a methanol and a 2-aminopyridinium cation. The electro-neutrality is reached between positive charges (copper ions and pyridinium moiety) and negative charges (**L1**, coordinated nitrates and hydroxide, free hydroxide). The structure shows a few supramolecular interactions that ensure the cohesion between building blocks. Indeed, three intramolecular and three inter-molecular H-bonds in addition to two intramolecular and three inter-molecular π–π interactions are found (Table S1).

*5.2.3. Crystal structure of **3***

The asymmetric part of the unit cell of **3**, which crystallizes in the triclinic space group $P\bar{1}$, contains a Ni^{II} dinuclear complex (Fig. 6). Each nickel ion sits in a distorted octahedral coordination sphere (distortion parameter [33], Σ_{Ni1} = 72°, Σ_{Ni2} = 60°) built from a methanol molecule, a linear isothiocyanato anion, a pyridine group originating from a terminal **L2H** as well as a pyridine, a μ-alkoxo and an imino group belonging to two different bridging **L2** ligands (Table 3). Two disordered methanol solvent molecules are also found in the crystal lattice. **L2** ligands are structurally different. Indeed, large differences are observed in the dihedral angle, between phenoxide and pyridine aromatic rings, as well as in the C7–N8–C9–C10 torsion angle allowed by the presence of the flexible methyl group (Table 1). Terminal **L2H** (**L2Ha** and **L2Hd**) are similar with dihedral angles of 60(1)° and 69(1)° and torsion angles of 125(1)° and 126(1)° although bridging **L2** (**L2b** and **L2c**) have dihedral angles of 76(1)° and 90(1)° and torsion angles of 97(1)°

Table 3
(a) Selected bond lengths (Å) and bond angles (°) for **1**–**3**.

1				**2**		**3**	
(a)							
Cu1–O16	2.267(3)	Cu3–O15	1.978(3)	Cu1–O202	2.28(1)	Ni1–N12	2.140(3)
Cu1–N1	2.026(3)	Cu3–O315	1.947(3)	Cu1–N1	2.016(8)	Ni1–N40	2.042(3)
Cu1–N107	2.005(3)	Cu4–O216	2.211(3)	Cu1–N107	2.001(7)	Ni1–N108	2.082(3)
Cu1–O115	1.941(3)	Cu4–N101	2.015(3)	Cu1–O15	1.965(5)	Ni1–N212	2.132(2)
Cu1–O215	1.981(3)	Cu4–N7	1.997(3)	Cu1–O115	1.942(6)	Ni1–O50	2.089(2)
Cu2–O116	2.341(5)	Cu4–O15	1.945(3)	Cu2–O20	2.167(7)	Ni1–O116	2.009(2)
Cu2–O119	2.786(3)	Cu4–O315	2.003(3)	Cu2–N7	1.997(7)	Ni2–N112	2.132(2)
Cu2–N301	2.031(3)	Cu5–O415	1.893(3)	Cu2–N101	2.024(8)	Ni2–N208	2.082(3)
Cu2–N207	2.012(3)	Cu5–N407	1.958(3)	Cu2–O15	1.948(6)	Ni2–N312	2.159(2)
Cu2–O115	1.998(3)	Cu5–O416	1.988(3)	Cu2–O115	1.980(6)	Ni2–N400	2.040(3)
Cu2–O215	1.947(3)	Cu5–O418	2.588(3)			Ni2–O216	2.021(2)
Cu3–O20	2.202(3)	Cu5–O516	2.010(3)			Ni2–O500	2.098(2)
Cu3–N201	2.021(3)	Cu5–O518	2.453(3)				
Cu3–N307	1.987(3)						

1						**2**		**3**			
(b)											
O16–Cu1–N1	93.5(1)	N301–Cu2–O115	99.4(1)	O216–Cu4–O15	93.5(1)	O202–Cu1–N1	92.7(3)	N40–Ni1–N108	94.1(1)	N208–Ni2–N400	93.9(1)
O16–Cu1–N107	85.3(1)	O115–Cu2–O215	75.2(1)	O216–Cu4–O315	91.9(1)	O202–Cu1–N107	84.4(4)	N108–Ni1–O116	91.1(1)	N400–Ni2–O500	89.3(1)
O16–Cu1–O115	92.5(1)	O20–Cu3–N201	93.9(1)	N7–Cu4–N101	94.9(1)	O202–Cu1–O15	122.8(4)	O116–Ni1–O50	84.4(1)	O500–Ni2–O216	87.3(1)
O16–Cu1–O215	119.4(1)	O20–Cu3–N307	101.8(1)	N101–Cu4–O315	98.4(1)	O202–Cu1–O115	91.5(3)	O50–Ni1–N40	90.3(1)	O216–Ni2–N208	89.5(1)
N1–Cu1–N107	94.8(1)	O20–Cu3–O15	97.0(1)	O315–Cu4–O15	75.4(1)	N1–Cu1–N107	95.4(3)	N12–Ni1–N40	91.6(1)	N112–Ni2–N208	91.6(1)
N107–Cu1–O115	88.6(1)	O20–Cu3–O315	90.0(1)	O15–Cu4–N7	88.5(1)	N107–Cu1–O115	89.4(3)	N12–Ni1–N108	90.6(1)	N112–Ni2–N400	93.2(1)
O115–Cu1–O215	75.8(1)	N201–Cu3–N307	94.5(1)	N407–Cu5–O415	92.8(1)	O115–Cu1–O15	75.4(2)	N12–Ni1–O116	86.8(1)	N112–Ni2–O500	90.8(1)
O215–Cu1–N1	98.6(1)	N307–Cu3–O315	88.9(1)	O415–Cu5–O416	88.0(1)	O15–Cu1–N1	98.5(3)	N12–Ni1–O50	88.2(1)	N112–Ni2–O216	87.3(1)
O116–Cu2–N301	89.4(1)	O315–Cu3–O15	76.0(1)	O416–Cu5–O516	89.7(1)	O20–Cu2–N7	101.1(3)	N212–Ni1–N40	92.6(1)	N312–Ni2–N208	89.0(1)
O116–Cu2–N207	123.2(1)	O15–Cu3–N201	99.2(1)	O516–Cu5–N407	91.6(1)	O20–Cu2–N101	96.8(3)	N212–Ni1–N108	89.4(1)	N312–Ni2–N400	93.6(1)
O116–Cu2–O115	87.2(1)	O216–Cu4–N7	122.7(1)	O418–Cu5–O416	54.6(1)	O20–Cu2–O15	89.3(3)	N212–Ni1–O50	91.5(1)	N312–Ni2–O216	85.8(1)
O116–Cu2–O215	93.1(1)	O216–Cu4–N101	89.6(1)	O518–Cu5–O516	57.0(1)	O20–Cu2–O115	101.7(3)	N212–Ni1–O116	89.1(1)	N312–Ni2–O500	88.2(1)
N207–Cu2–N301	94.7(1)					N7–Cu2–N101	95.7(3)	Ni1–N40–C41	175.7(1)	Ni2–N400–C401	171.4(1)
						N101–Cu2–O115	97.9(3)	N40–C41–S42	178.1(1)	N400–C401–S403	179.2(1)
						O115–Cu2–O15	74.9(2)				
						O15–Cu2–N7	89.0(3)				

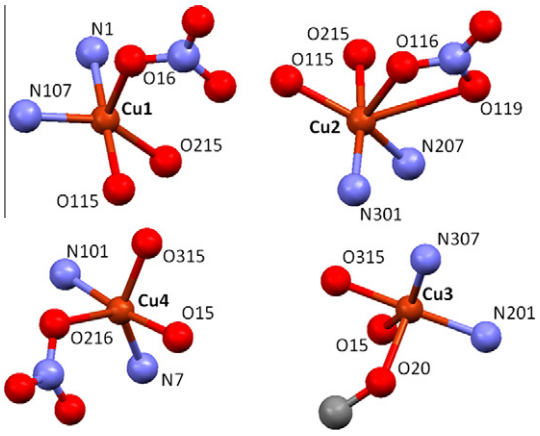

Fig. 2. View of the coordination spheres in the tetranuclear unit of **1**.

and 109(1)°. A larger metal distance (6.758(3) Å) is observed compared to the ones found for **1** and **2** (Table 2). This difference originates from the presence of a methyl group spacer in the related donor ligand **L2H**. The dinuclear motif is slightly asymmetric as confirmed by the bond lengths differences noted in the coordination spheres of Ni1 and Ni2 (Table 3) and presents a helicate geometry provided by the **L2** torsion angle. A racemic mixture of left (Λ) and right hand (Δ) enantiomers that are generated by symmetry within the centrosymmetric $P\bar{1}$ space group. The structure is also characterised by a supramolecular interactions network. Indeed, three intramolecular H-bonds and one intramolecular π–π stacking interaction ensure the stability and the geometry of the supramolecular architecture. In addition to the intramolecular interactions, the cohesion between the dinuclear units and between complexes and guest molecules is obtained by three inter-molecular H-bonds and three π–π stacking interactions (Table S1).

5.3. Magnetic properties

The magnetic properties of a polycrystalline sample of **1** were measured over the 1.8–300 K range, with an applied magnetic field

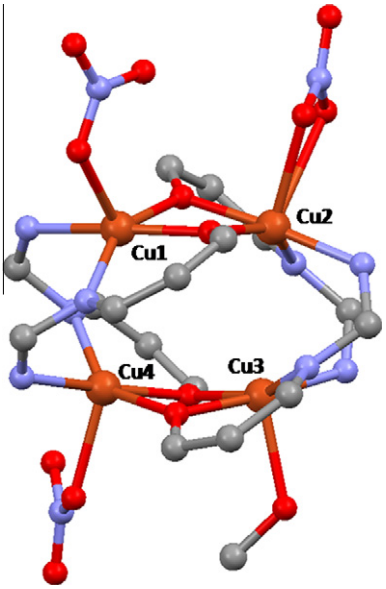

Fig. 3. View of the magnetic pathways in **1**, between the magnetic dinuclear units (Cu1, Cu2) and (Cu3, Cu4).

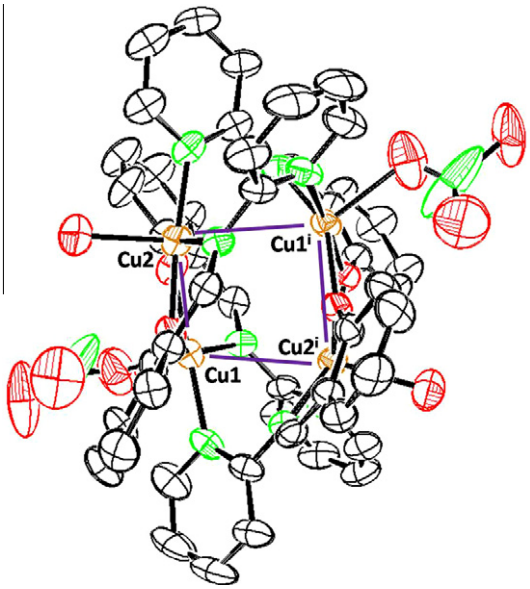

Fig. 5. ORTEP view of the tetranuclear unit (violet square) in **2**, showing 50% probability displacement ellipsoids. H atoms and guest molecules were omitted for clarity.

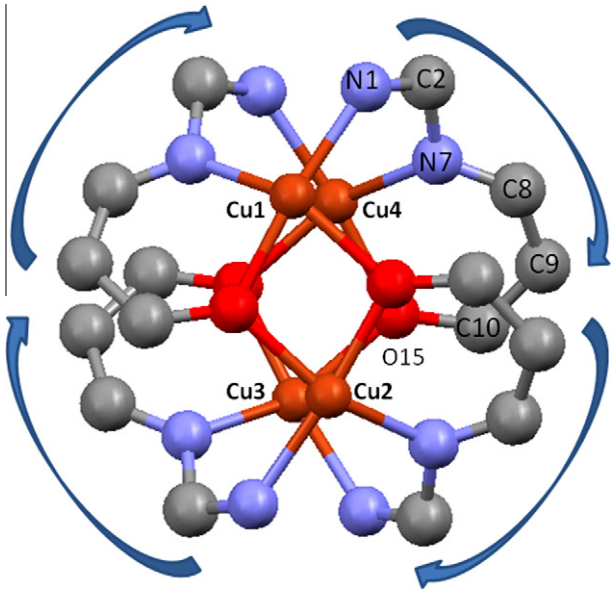

Fig. 4. View of the tetranuclear core of **1** revealing a right hand quadruple helicate structure thanks to the torsion of four **L1** ligands. The arrows indicate the clockwise rotation, e.g. from Cu1 (top) to Cu3 (bottom) following the labeled sequence. A similar view can be depicted for **2**.

of 1000 Oe. At room temperature, χT was 0.63 $cm^3\,K\,mol^{-1}$ that is far from the theoretical value of 1.875 $cm^3\,K\,mol^{-1}$, which is expected for five isolated paramagnetic Cu(II) ions (d^9, $S = 1/2$) with $g = 2$. This behaviour indicates that dominant anti-ferromagnetic (AF) exchange interactions exist between the Cu(II) ions which are confirmed on cooling by the continuous decrease of the χT product that reaches a value around 0.40 $cm^3\,K\,mol^{-1}$ below 100 K. This value is in good agreement with the residual magnetism coming from the mononuclear Cu(II) $S = 1/2$ unit. As shown in the crystal analysis, complex **1** can be topologically viewed as two dinuclear moieties composed of two $S = 1/2$ Cu(II) ions (Fig. 3) [34]. The magnetic data have been thus approximately modeled using an isotropic Heisenberg $S = 1/2$ dimer model and the following Hamiltonian:

$$H = -2J(S_{CuA} \cdot S_{CuB})$$

where J is the average exchange interaction within dinuclear Cu units: Cu1–Cu2 and Cu3–Cu4 that are considered identical in this simplified approach; S_i the spin operators for each centres. The application of the van Vleck equation [35a] to the Kambe's vector coupling scheme [35b], allows a determination of the low field analytical expression of the magnetic susceptibility [35c] taking into account the presence of the residual $S = 1/2$ mononuclear unit:

$$\chi T = \frac{4Ng^2\mu_B^2}{k_B}\frac{1}{3+\exp\left(\frac{-2J}{k_BT}\right)} + \frac{Ng^2\mu_B^2}{4k_B}$$

This approximated model reproduces rather well the experimental results over the 1.5–300 K range as shown in Fig. 7. The best set of parameters are $g = 2.06(3)$ and $J/k_B = -489(3)$ K ($J = -340(2)\,cm^{-1}$). The sign of the magnetic interaction implies that these copper binuclear units and thus the tetramer complex possesses a $S_T = 0$ ground state.

It is worth mentioning that two other analyses of the magnetic data have been attempted: (i) considering two different dinuclear moieties with two independent magnetic interactions and (ii) considering identical dinuclear units that possess inter-dimer magnetic interactions through the N–C–N bridges. While the first approach leads to identical magnetic intra-dimer interactions and thus the same result displayed in Fig. 7, the second model converges to an unphysically large value of the inter-dimer interaction (of the order of the intra-dimer interactions). Therefore, we assume that the inter-binuclear magnetic coupling is too weak in comparison to the intra-dimer interactions to be correctly estimated. The magnetic properties of the related grid **4** support an AF exchange interactions between Cu(II) ions [31], but no comparison can be made due to severe uncertainties both in the fit and acquisition of magnetic data (contamination of diamagnetic impurities) in [31].

6. Discussion

Reacting a Cu(II) salt with **L1H** in methanol afforded tetranuclear [2 × 2] grid-like complexes (**1** and **2**). The composition of

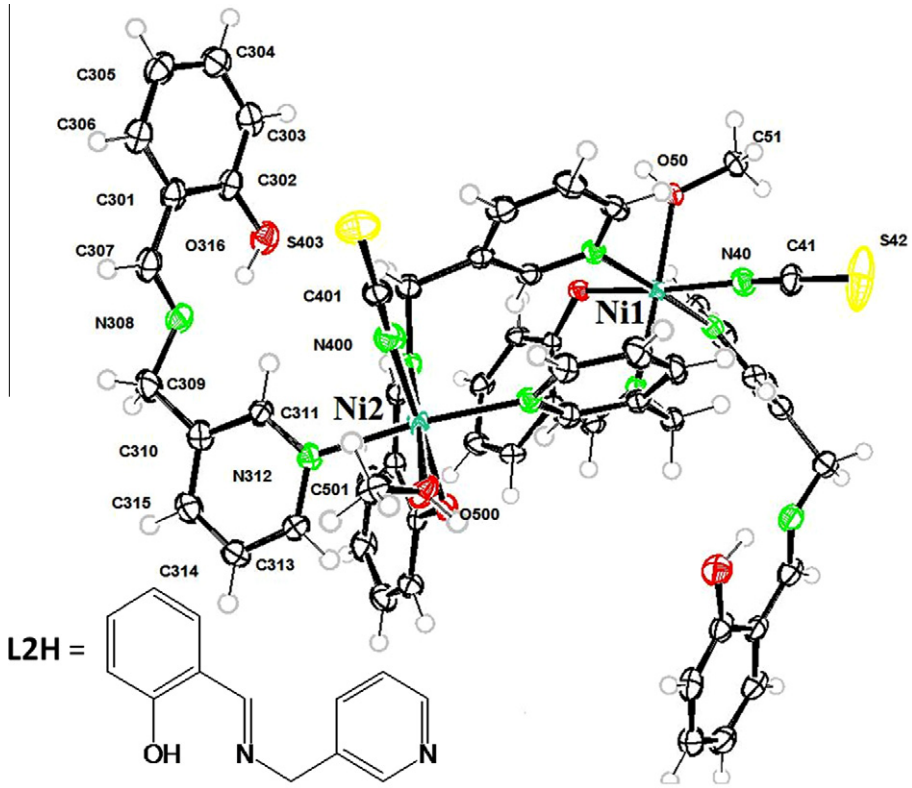

Fig. 6. ORTEP view of the asymmetric part of the unit cell for **3**, showing 50% probability displacement ellipsoids. The two solvent methanol molecules were omitted for clarity. The inset shows a scheme of the **L2H** ligand.

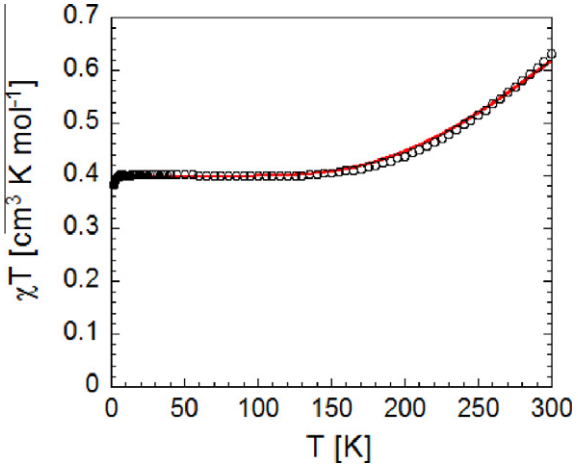

Fig. 7. Temperature dependence of χT for **1** at 1000 Oe (with χ defined as M/H). The open dots indicate the experimental data points and the line represents the best fitting curve obtained with the Heisenberg model described in the text.

these complexes is different from the one reported by Hatfield [36] and Drummond [31] which was obtained following a different synthetic method in isopropanol. Indeed, Ref. [31] reports on a highly symmetric tetranuclear complex $[Cu_4(\mathbf{L1})_4(H_2O)_4](NO_3)_4$ (**4**) (as shown by the $P4_22_12$ space group) where all Cu(II) ions are identical and generated by symmetry). In **1**, three Cu(II) coordination spheres with two distinct geometries around metal ions were identified, whereas two types of coordination spheres and two different **L1** ligands (**L1a**–**b**) were identified for **2**. Such an asymmetry is not only visible in Cu^{II} coordination spheres (Table 3) but also in ligands, which can be differentiated by their dihedral angles Φ (Table 1). This structural feature provides chirality to the tetranuclear unit thanks to a **L1** torsion angle of approximately 40° (Table 1). The same structural feature is present in **4** but it was not discussed in [31]. In addition to the depicted 'intramolecular asymmetry', the inter-molecular interactions network appears also to be asymmetric in **1**. Such a network is less dense in the centrosymmetric tetranuclear **2**. The difficulty to isolate **2** in large amount compared to **1** may stem from the dense supramolecular network (Table S1), developed in **1**, which strongly stabilizes the structure and thus eases the crystallization. Comparison with the network developed in **4** is not feasible because the deposited CIF file in [31] does not contain any nitrato anions due to disorder [31].

As seen in the crystal structures, the tetranuclear assembly is built by connecting two dinuclear units by a double N–C–N bridge, with short Cu···Cu distances (~3 Å) (Fig. 3) allowing a strong AF coupling as revealed by the study of the magnetic properties ($J = -340(2)\ cm^{-1}$) for **1**. This coupling constant reaches the same order of magnitude than observed for a related [4 × 4] grid-like complex ($J = -271\ cm^{-1}$) [37]. Interestingly, the position in the Cu^{II} coordination spheres, occupied by the nitrato anion and methanol molecules in **1** and by methanol and hydroxide molecules in **2**, can be considered as labile. It suggests that a large variety of molecules may be formed in solution but that a selective crystallization of more stable complexes has occurred affording **1** and **2**. In this scheme, the influence of the synthetic solvent could explain the large composition and structural differences with respect to **4** [31]. Interestingly, an intermediate mononuclear compound was also isolated in the crystal lattice of **1**. Because of the apparent complexity of the crystal structures of **1** and **2**, we have investigated the coordination chemistry with another related ligand, **L2H**, which has a flexible methyl group between aromatic rings, in order to block the formation of tetranuclear units at a lower nuclearity stage. To reach this goal, a nickel ion in combination with a thiocyanato anion were selected and afforded the dinuclear

complex **3**. Even though the systems **1**–**2** and **3** are quite different, we observe the formation of a similar framework involving all donor atoms present in **L1** and **L2**. Taking into account that both dinuclear units in **1** and **2** are linked by two N–C–N bridges, here the dinuclear moiety **3** is linked by two N–C–C–C–N bridges (Fig. 6). This compound completes the short list of crystal structures of nickel dinuclear complexes with N–C_x–N bridges [38]. Interestingly, this bridging configuration imitates rather well the lateral side of the grid in **1** and **2** (Fig. 3). Bridging ligands **L2b** and **L2c** in **3** are indeed similar than **L1a** and **L1b** in **1** except that the alkoxo group, that was bidentate, becomes monodentate. The bridge between metal ions is longer in **3** than in **1** and **2** (6.758(3) Å compared to 3.2–3.3 Å – Table 1) because of the methyl spacer group in **L2**. The fact that a **L2H** ligand is found in **3** is rather interesting taking into account that *N*-salicylidene aminopyridine complexes have recently shown to present switchable chromic properties [39]. This is for instance the case for the mononuclear complex, $[Ni(CH_3OH)_2(\mathbf{L4H})_2(NCS)_2]$ with **L4H** = *N*-salicylidene-3-aminopyridine, that presents weak thermochromism on cooling below room temperature [39]. The studies of optical properties of **3**, that was beyond the scope of this study, should be considered in the near future.

7. Concluding remarks

We have described a remarkable asymmetric Cu(II) [2 × 2] grid-like complex (**1**). This tetranuclear unit, which reveals a strong AF coupling between dinuclear units through a double alkoxo bridge, is embedded in a sophisticated supramolecular network. Complexes **2** and **4** represent other examples of tetranuclear grids formed with the same ligand. The use of such Schiff base ligands thus open perspectives into developing magnetic asymmetric coordination units.

Acknowledgments

This work was partly funded by the Fonds National de la Recherche Scientifique-FNRS (FRFC N°2.4508.08), the Interuniversity attraction pole IAP-VI (P6/17) INANOMAT program, a Concerted Research Action of the "Communauté Française de Belgique" allotted by the Académie Universitaire Louvain, MAGMANet (NMP3-CT-2005-515767), the University of Bordeaux, the CNRS, the GIS Advanced Materials in Aquitaine (COMET Project) and the Région Aquitaine. We also thank the Fonds pour la Formation à la Recherche dans l'Industrie et dans l'Agriculture for a doctoral scholarship allocated to F.R.

Appendix A. Supplementary data

CCDC 732107, 749405 and 749404 contain the supplementary crystallographic data for **1**, **2** and **3**, respectively. These data can be obtained free of charge via http://www.ccdc.cam.ac.uk/conts/retrieving.html, or from the Cambridge Crystallographic Data Centre, 12 Union Road, Cambridge CB2 1EZ, UK; fax: (+44) 1223-336-033; or e-mail: deposit@ccdc.cam.ac.uk. Supplementary data associated with this article can be found, in the online version, at doi:10.1016/j.poly.2010.06.017.

References

[1] G.R. Desiraju, Angew. Chem., Int. Ed. 46 (2007) 8342.
[2] (a) G. Hanan, C. Arana, J.-M. Lehn, D. Fenske, Angew. Chem., Int. Ed. Engl. (1995) 1122;
(b) H. Sleiman, P.N.W. Baxter, J.-M. Lehn, K. Rissanen, J. Chem. Soc., Chem. Commun. (1995) 715;
(c) H. Sleiman, P.N.W. Baxter, J.-M. Lehn, K. Airola, K. Rissanen, Inorg. Chem. 3 (1997) 4734.
[3] P.N.W. Baxter, J.-M. Lehn, A. De Cian, J. Fischer, Angew. Chem., Int. Ed. Engl. 32 (1993) 69.
[4] P.N.W. Baxter, J.-M. Lehn, J. Fischer, M.-T. Youinou, Angew. Chem., Int. Ed. Engl. 33 (1994) 2284.
[5] M. Barboiu, E. Petit, A. van der Lee, G. Vaughan, Inorg. Chem. 45 (2006) 484.
[6] (a) L.N. Dawe, L.K. Thompson, Angew. Chem., Int. Ed. 46 (2007) 7440;
(b) L.N. Dawe, K.V. Shuvaev, L.K. Thompson, Inorg. Chem. 48 (2009) 3323.
[7] (a) J.I. van der Vlugt, S. Demeshko, S. Dechert, F. Meyer, Inorg. Chem. 47 (2008) 1576;
(b) Y.S. Moroz, K. Kulon, M. Haukka, E. Gumienna-Kontecka, H. Kozłowski, F. Meyer, I.O. Fritsky, Inorg. Chem. 47 (2008) 5656.
[8] T. Weilandt, R.W. Troff, H. Saxell, K. Rissanen, C.A. Schalley, Inorg. Chem. 47 (2008) 7588.
[9] K. Yamauchi, Y. Takashima, A. Hashidzume, H. Yamaguchi, A. Harada, J. Am. Chem. Soc. 130 (2008) 5024.
[10] Z. Ge, J. Hu, F. Huang, S. Liu, Angew. Chem., Int. Ed. 48 (2009) 1798.
[11] U. Ziener, J.-M. Lehn, A. Mourran, M. Moller, Chem. Eur. J. 8 (2002) 951.
[12] M. Ruben, J. Rojo, F.J. Romero-Salguero, L.H. Uppadine, Angew. Chem., Int. Ed. 43 (2004) 3644.
[13] O. Roubeau, R. Clérac, Eur. J. Inorg. Chem. 28 (2008) 4325.
[14] (a) E. Breuning, M. Ruben, J.-M. Lehn, F. Renz, Y. Garcia, V. Ksenofontov, P. Gütlich, E. Wegelius, K. Rissanen, Angew. Chem., Int. Ed. 39 (2000) 2504;
(b) M. Ruben, E. Breuning, J.-M. Lehn, V. Ksenofontov, F. Renz, P. Gütlich, G.B.M. Vaughan, Chem. Eur. J. 9 (2003) 4422;
(c) M. Ruben, U. Ziener, J.-M. Lehn, V. Ksenofontov, P. Gütlich, G.B.M. Vaughan, Chem. Eur. J. 11 (2004) 94;
(d) M. Ruben, E. Breuning, J.-M. Lehn, V. Ksenofontov, P. Gütlich, G. Vaughan, J. Magn. Magn. Mater. 272–276 (2004) e715;
(e) A.R. Stefankiewicz, J.-M. Lehn, Chem. Eur. J. 15 (2009) 2500.
[15] A.K. Boudalis, C.P. Raptopoulou, V. Psycharis, B. Abarca, R. Ballesteros, Eur. J. Inorg. Chem. 24 (2008) 3796.
[16] L.K. Thompson, Coord. Chem. Rev. 233–234 (2002) 193.
[17] (a) B. Graham, M.T.W. Hearn, P.C. Junk, C.M. Kepert, F.E. Mabbs, B. Moubaraki, K.S. Murray, L. Spiccia, Inorg. Chem. 40 (2001) 1536;
(b) K.L.V. Mann, E. Psillakis, J.C. Jeffery, L.H. Rees, N.M. Harden, J.A. McCleverty, M.D. Ward, D. Gatteschi, F. Totti, F.E. Mabbs, E.J.L. McInnes, P.C. Riedi, G.M. Smith, J. Chem. Soc., Dalton Trans. (1999) 339.
[18] R.H. Holm, P. Kennepohl, E.I. Solomon, Chem. Rev. 96 (1996) 2239.
[19] V. Chandrasekhar, L. Nagarajan, R. Clérac, S. Ghosh, S. Verma, Inorg. Chem. 47 (2008) 1067.
[20] G.L.J.A. Rikken, E. Raupauch, Nature 390 (1997) 493.
[21] L.D. Barron, Nat. Mater. 7 (2008) 691.
[22] A. von Zelewsky, Stereochemistry of Coordination Compounds, John Wiley and Sons, Chichester, 1996.
[23] V.I. Sokolov, Chiral and Optical Activity in Organometallic Compounds, Gordon and Breach Science Publishers, New York, 1990.
[24] J. Crassous, Chem. Soc. Rev. 38 (2009) 830.
[25] A. Fragoso, M.L. Kahn, A. Castiñeiras, J.P. Sutter, O. Kahn, R. Cao, Chem. Commun. (2000) 1547.
[26] (a) S.J. Loeb, C.J. Willis, Inorg. Chem. 20 (1981) 2791;
(b) A. Burkhardt, E.T. Spielberg, H. Görls, W. Plass, Inorg. Chem. 47 (2008) 2485;
(c) L.-L. Fan, F.-S. Guo, L. Yun, Z.-J. Lin, R. Herchel, J.-D. Leng, Y.-C. Ou, M.-L. Tong, Dalton Trans. 39 (2010) 1771.
[27] W.E. Hatfield, F.L. Bunger, Inorg. Chem. 8 (1969) 1194.
[28] E. Hadjoudis, J. Petrou, J. Xexakis, Mol. Cryst. Liq. Cryst. 93 (1983) 73.
[29] G.M. Sheldrick, SHELX97: Program System for Crystal Structure Determination, University of Göttingen, Germany, 1997.
[30] A.W. Addison, T.N. Rao, J. Reedijk, J. Van Rijn, G.C. Verschoor, Chem. Soc., Dalton Trans. (1984) 1349.
[31] J. Drummond, J.S. Wood, J. Chem. Soc., Dalton Trans. 3 (1972) 365.
[32] M. Albrecht, Chem. Rev. 101 (2001) 3457.
[33] P. Guionneau, M. Marchivie, G. Bravic, J.-F. Létard, D. Chasseau, Top. Curr. Chem. 234 (2004) 97.
[34] J.E. Andrew, A.B. Blake, L.R. Fraser, J. Chem. Soc., Dalton Trans. (1976) 477.
[35] (a) J.H. van Vleck, in: The Theory of Electric and Magnetic Susceptibility Oxford University Press, 1932.;
(b) K.J. Kambe, Phys. Soc. Jpn. 5 (1950) 48;
(c) C.J. O'Connor, Prog. Inorg. Chem. 29 (1982) 203.
[36] W.E. Hatfield, F.L. Bunger, Inorg. Chem. 8 (1969) 1194.
[37] S. Gou, M. Qian, Z. Yu, C. Duan, X. Sun, W.J. Huang, J. Chem. Soc., Dalton Trans. (2001) 3232.
[38] (a) L.-P. Lu, X.-P. Lu, M.-L. Zhu, Acta Crystallogr., Sect. C 63 (2007) m374;
A.R. Paital, M. Mikuriya, D. Ray, Eur. J. Inorg. Chem. (2007) 5360;
(c) S.V. Larionov, T.E. Kokina, L.A. Glinskaya, R.F. Klevtsova, Coord. Chim. 28 (2002) 597;
(d) A.R. Paital, W.T. Wong, G. Aromi, D. Ray, Inorg. Chem. 46 (2007) 5727;
(e) M. Fondo, N. Ocampo, A.M. Garcia-Deibe, R. Vincente, M. Corbella, M.R. Bermejo, J. Sanmartin, Inorg. Chem. 45 (2006) 255;
(f) C.H. Ng, T.S. Chong, S.G. Teoh, S.W. Ng, J. Coord. Chem. 58 (2005) 1455;
(g) M. Fondo, A.M. Garcia-Deibe, N. Ocampo, J. Sanmartin, M.R. Bermejo, A.L. Llamas-Saiz, Dalton Trans. (2006) 4260;
(h) M. Fondo, A.M. Garcia-Deibe, N. Ocampo, J. Sanmartin, M.R. Bermejo, Dalton Trans. (2007) 414.
[39] F. Robert, A.D. Naik, B. Tinant, R. Robiette, Y. Garcia, Chem. Eur. J. 15 (2009) 4327.